Ergodicity Breaking Transition in Zero Dimensions

Jan Šuntajs and Lev Vidmar
Department of Theoretical Physics, J. Stefan Institute, SI-1000 Ljubljana, Slovenia
and Department of Physics, Faculty of Mathematics and Physics, University of Ljubljana, SI-1000 Ljubljana, Slovenia

(Received 22 March 2022; accepted 11 July 2022; published 5 August 2022)

It is of great current interest to establish toy models of ergodicity breaking transitions in quantum many-body systems. Here, we study a model that is expected to exhibit an ergodic to nonergodic transition in the thermodynamic limit upon tuning the coupling between an ergodic quantum dot and distant particles with spin-1/2. The model is effectively zero dimensional; however, a variant of the model was proposed by De Roeck and Huveneers to describe the avalanche mechanism of ergodicity breaking transition in one-dimensional disordered spin chains. We show that exact numerical results based on the spectral form factor calculation accurately agree with theoretical predictions, and hence unambiguously confirm existence of the ergodicity breaking transition in this model. We benchmark specific properties that represent hallmarks of the ergodicity breaking transition in finite systems.

DOI: 10.1103/PhysRevLett.129.060602

Introduction.—A fascinating property of isolated interacting quantum many-body systems is their ability to thermalize. This statement usually refers to the properties of local observables [1–8], while many generic properties of ergodic systems can often be understood by analyzing statistical properties of their energy spectra and comparing them to the predictions of random matrix theory [5,9].

Nevertheless, it was shown experimentally already more than 15 years ago that isolated interacting quantum many-body systems may not always thermalize [10], at least on the experimentally relevant timescales [10–14]. One class of interacting quantum systems exhibiting absence of thermalization and nonergodic dynamics are integrable systems, the spin-1/2 Heisenberg chain with translational invariance being a paradigmatic example [15–18]. However, it is likely that in the thermodynamic limit, nonergodicity in these systems is not robust against adding small integrability breaking terms [19–28]. It is therefore of great scientific interest to uncover other classes of interacting quantum systems that exhibit robust counterexamples to thermalization. Perhaps the most fascinating property of such systems would be the emergence of an ergodicity breaking phase transition between an ergodic and a nonergodic phase.

Recent experimental activities have led to demonstrations of different fingerprints of potentially robust nonergodic dynamics in interacting quantum systems at experimentally accessible times [29–33]. From the theoretical perspective, however, it remains far from clear what are the universal properties of ergodicity breaking transitions, which are the relevant toy models, and what tools should one apply to detect the transition.

The latter statement may be illustrated by the example of a possible ergodicity breaking in spin-1/2 chains in random magnetic fields that act as quenched disorder. It was proposed that such systems, which are ergodic at weak disorder, undergo an ergodicity breaking phase transition upon increasing the disorder [34]. While the fate of this transition in the thermodynamic limit is still under debate [35–52], it was noticed that many properties of finite systems at rather large disorder appear to be nonergodic; however they may eventually become ergodic in the thermodynamic limit [35]. This perspective has been then further supported using various different theoretical and numerical arguments [39–41,53–55].

Based on the above arguments, it appears crucial to establish generic toy models of ergodicity breaking transitions, for which theoretical predictions and exact numerical results agree both qualitatively and quantitatively. In this Letter, we achieve this goal for an interacting

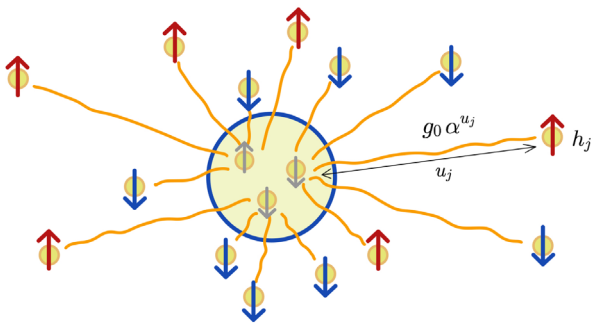

FIG. 1. Sketch of the model from Eq. (1). Interactions of particles within the dot (blue circle) are described by a random matrix. A particle j outside the dot experiences the magnetic field h_j, and its distance from the dot is u_j. The coupling amplitude between a particle j and a randomly selected particle in the dot is $g_0\alpha^{u_j}$.

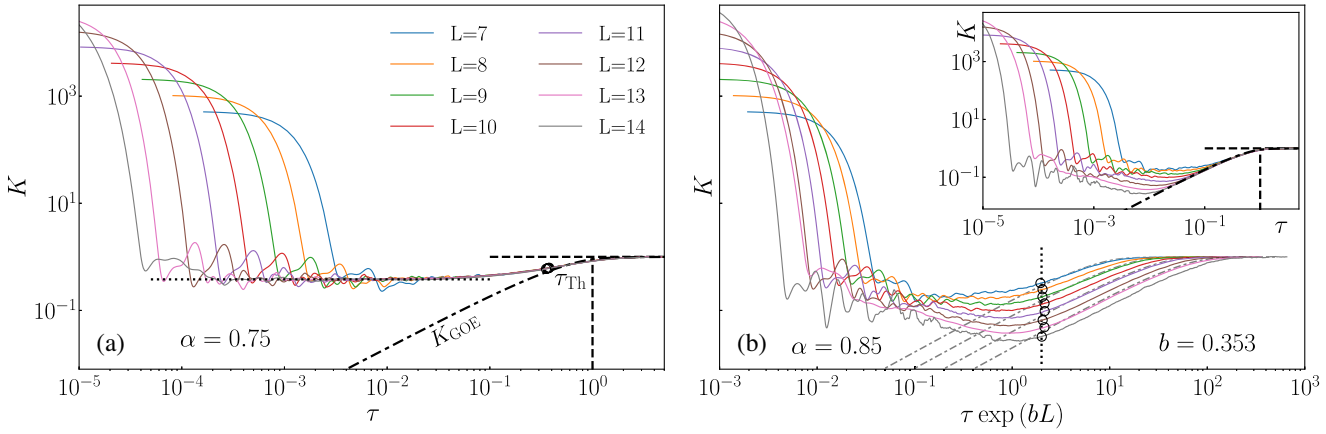

FIG. 2. Spectral form factor $K(\tau)$ at different system sizes L. Dashed-dotted lines denote the GOE results $K_{\mathrm{GOE}}(\tau) = 2\tau - \tau\ln(1+2\tau)$, open circles denote the extracted values of τ_{Th}, and the vertical dashed line is the scaled Heisenberg time $\tau_H = 1$. (a) $K(\tau)$ at $\alpha = \alpha_c = 0.75$. The horizontal dotted line is the fit $K(\tau) \approx 0.38$. (b) $K(\tau)$ at $\alpha = 0.85$. The inset shows the raw data while in the main panel we rescale $\tau \to \tau\exp(bL)$, where $b = 0.353$, such that the rescaled values of τ_{Th} coincide. See [57] for a detailed description of the numerical extraction of τ_{Th}.

zero-dimensional model sketched in Fig. 1, which is expected to exhibit features of the avalanche mechanism introduced by De Roeck and Huveneers [56]. Based on the spectral form factor (SFF) analysis, we benchmark several properties of the ergodicity breaking transition, such as (a) signatures of a universal SFF shape at the transition point, (b) exponential dependence of the Thouless time on both the system size and the interaction, which can be detected already deep in the ergodic regime, and (c) extraction of a diverging length scale at the transition. We argue that these properties may represent hallmarks of an ergodicity breaking transition (EBT) in finite systems.

Model.—We study a model of spin-1/2 particles that consists of two subsystems, as sketched in Fig. 1: a subsystem of N particles with all-to-all interactions (referred to as a "dot"), and a subsystem of L particles outside the dot, where each particle is only coupled to a single particle within the dot. The full model Hamiltonian reads

$$\hat{H} = R + \sum_{j=1}^{L} g_0 \alpha^{u_j} \hat{S}^x_{n_j} \hat{S}^x_j + \sum_{j=1}^{L} h_j \hat{S}^z_j. \tag{1}$$

Properties of N particles within the dot are described by a $2^N \times 2^N$ random matrix R drawn from the Gaussian orthogonal ensemble (GOE) that acts nontrivially on dot's degrees of freedom only. The fields h_j that act on particles outside the dot are drawn from a random box distribution, $h_j \in [0.5, 1.5]$. In the coupling term, $\hat{S}^x_{n_j}$ acts on a randomly selected site n_j within the dot, while $\hat{S}^x_j$ acts on the particle j outside the dot. The tuning parameter of the coupling strength $g_0\alpha^{u_j}$ is the parameter α (we set $g_0 \equiv 1$), while u_j represents the distance between a coupled particle and the dot. The latter is sampled from a random box distribution $u_j \in [j - \zeta_j, j + \zeta_j]$. Apart from the energy conservation, the system has no other conservation laws and its corresponding total Hilbert space dimension equals $\mathcal{D} = 2^{N+L}$. We set $N = 3$ and $\zeta_j = 0.2$ throughout the study (see [57] for details).

A similar version of the model was used in Refs. [56,61,62] in the description of the avalanche mechanism in one-dimensional (1D) strongly disordered spin chains, and a related model was studied in Ref. [63] to shed light on instability of nonergodicity in higher dimensions. Here, we argue that the model [Eq. (1)] is a zero-dimensional model since the thermodynamic limit is obtained by sending the number of particles outside the dot $L \to \infty$ while their coordination number $z = 1$, and the number of particles within the dot N are fixed. Accordingly, we treat the model as a toy model to describe the EBT in zero dimensions and steer away from making any predictions regarding 1D (or higher-D) systems.

Spectral form factor (SFF).—The central quantity in our study is the SFF $K(\tau)$, which is the Fourier transform of the two-point spectral correlations, defined as

$$K(\tau) = \frac{1}{Z}\left\langle \left| \sum_{n=1}^{\mathcal{D}} \rho(\varepsilon_n) e^{-i2\pi\varepsilon_n\tau} \right|^2 \right\rangle. \tag{2}$$

Here, $\{\varepsilon_1 \le \varepsilon_2 \le \cdots \varepsilon_{\mathcal{D}}\}$ is the complete set of Hamiltonian eigenvalues after spectral unfolding, τ is the scaled time, and the average $\langle \ldots \rangle$ is carried out over different realizations of $\hat{H}$. We follow the implementation of $K(\tau)$ from [35], which is for convenience summarized in the Supplemental Material [57] (the normalization Z and a smooth filtering function $\rho(\varepsilon_n)$ that eliminates contributions of the spectral edges are provided there). Numerically, we study systems with up to $L + N = 17$ sites, thus requiring full exact diagonalization of matrices up to dimension $\mathcal{D} \times \mathcal{D}$, where $\mathcal{D} = 2^{17} = 131072$.

Our main intuition for why the SFF should represent a useful tool to detect the EBT is based on the analysis of the localization transition in the three-dimensional (3D) Anderson model [64], for which the transition point is known to high accuracy [64,65]. At the transition point in the 3D Anderson model, $K(\tau)$ exhibits a universal shape that is independent of the system size for a wide interval of τ, and it consists of two regimes [64]: $K(t) \approx \text{const}$ at $\tau \ll 1$, followed by a short interval around $\tau \lesssim 1$ where $K(\tau) \approx K_{\text{GOE}}(\tau) = 2\tau - \tau \ln(1 + 2\tau)$. We define the Thouless time τ_{Th} (in scaled units) as the time when the SFF $K(\tau)$ approaches the GOE prediction $K_{\text{GOE}}(\tau)$. If $K(\tau)$ is universal and independent of system size L, the same holds true for τ_{Th}. One can hence consider independence of τ_{Th} on L as a criterion for the transition.

Remarkably, a very similar structure of $K(\tau)$ is also observed in the model from Eq. (1), which is shown in Fig. 2(a) at $\alpha = 0.75$. At this value of α, $K(\tau)$ appears to exhibit the most L-independent form (apart from the short time limit $\tau \to 0$ when $K(\tau) \gg 1$). The value of $K(\tau)$ in the broad τ-independent regime is $K(\tau) \approx 0.38$, which is very close to the one in the 3D Anderson model at the transition point (cf. Fig. 8(a) in [64]).

Before proceeding, we note that our results suggest the EBT to occur at $\alpha \approx 0.75$, and hence we set $\alpha_c = 0.75$ further on. Some analytical arguments (to be presented below and also in [56,61]) predict the transition to occur at $\bar{\alpha} = 1/\sqrt{2} \approx 0.71$. While our numerical results are not inconsistent with the latter prediction, we also refrain from making any sharp predictions of the transition point in systems much larger than those studied here, or in systems with a different choice of model parameters.

Figure 2(b) displays results for $K(\tau)$ in the ergodic regime at $\alpha = 0.85$. In the inset we show that $\tau_{\text{Th}} \to 0$ in the thermodynamic limit $L \to \infty$, which can be seen as a hallmark of ergodicity. The most remarkable property of $K(\tau)$ can be observed when the scaled time τ is multiplied by a factor $\exp(bL)$, where b is a constant. Results shown in the main panel of Fig. 2(b) suggest that after this rescaling, the Thouless time becomes nearly independent of L. This indicates that the Thouless time in physical units scales exponentially with L in the ergodic regime, and will be analyzed in more detail below.

Thouless time in the ergodic regime.—From now on we consider the Thouless time in physical units, which is defined as $t_{\text{Th}} = \tau_{\text{Th}} \hbar / \overline{\delta E}$, where $\overline{\delta E}$ is the mean level spacing [57] and we set $\hbar \equiv 1$. In Fig. 3(a), we show t_{Th} versus L in a log-linear scale at different α in the ergodic regime, and at $\alpha = \alpha_c$. The results suggest that t_{Th} increases exponentially with L, at least in the regime $\alpha \lesssim 0.87$. This is corroborated in the inset of Fig. 3(b) where the same results are shown on a log-log scale, exhibiting a growth with L that is faster than power law. We describe these results with the ansatz

$$t_{\text{Th}} \propto e^{fL}. \tag{3}$$

An important property of this ansatz is that $f = f(\alpha)$ is a function of the coupling strength, as evident from the varying slopes of $t_{\text{Th}}(L)$ in a log-linear scale in Fig. 3(a). The dashed-dotted line in Fig. 3(a) denotes the scaling with L of the Heisenberg time $t_H = 1/\overline{\delta E}$, which has the same slope as $t_{\text{Th}}(L)$ at $\alpha = \alpha_c$.

We can explain the relation in Eq. (3) by a rather crude and simple approximation, which is however accurate enough for building our intuition about the key scaling relations in the system. Since t_{Th} may be seen as the longest physically relevant timescale, we estimate its inverse, denoted E^*_{Th}, by the coupling of the farthermost particle to the dot, $g_L = \alpha^L$. Using the Fermi golden rule arguments, one gets $E^*_{\text{Th}} = g_L^2/\varepsilon$, where $\varepsilon = \mathcal{O}(1)$ [61]. Then, $t^*_{\text{Th}} = 1/E^*_{\text{Th}}$ is given by

$$t^*_{\text{Th}} \propto \alpha^{-2L} = e^{\ln(\frac{1}{\alpha^2})L}. \tag{4}$$

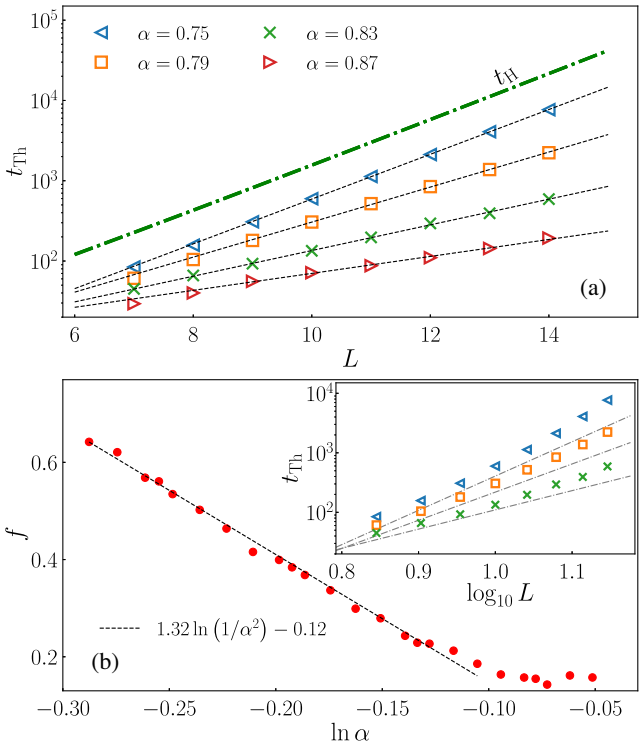

FIG. 3. (a) Scaling of the Thouless time t_{Th} with L on a log-linear scale for different values of α (symbols). Dashed lines are fits to Eq. (3), while the dashed-dotted line is the scaling of the Heisenberg time t_H. The same results are shown in the inset of (b) on a log-log scale, where dashed-dotted lines are guides to the eye with the same slope as the power-law fits to the numerical data. (b) Dependence of f on $\ln \alpha$, where f is obtained by fitting Eq. (3) to the results for $t_{\text{Th}}(L)$. Line is the fitted function $f(\alpha) = 1.32 \ln(1/\alpha^2) - 0.12$.

In the main panel of Fig. 3(b) we plot the rates f, obtained by fitting Eq. (3) to the actual numerical results, versus $\ln\alpha$. We fit the ansatz $f(\alpha) = a_1 \ln(1/\alpha^2) + a_0$ to the results in the interval $\alpha \in [0.75, 0.87]$, and get $a_1 = 1.32$, $a_0 = -0.12$. This is indeed reasonably close to the prediction by Eq. (4), $f(\alpha) = \ln(1/\alpha^2)$, which assumes $a_1 = 1$ and $a_0 = 0$.

Criterion for the EBT.—We next discuss the connection of the results presented so far with the emergence of EBT. We expect that the system is ergodic when the Thouless time t_{Th} increases slower than the Heisenberg time $t_H \propto 2^L = e^{\ln(1/\bar{\alpha}^2)L}$, where $\bar{\alpha} = 1/\sqrt{2}$, while the onset of nonergodic behavior occurs when both times scale identically. This gives rise to the criterion for the EBT

$$\frac{t_H}{t_{\mathrm{Th}}} = \text{const.} \tag{5}$$

As argued in our discussion of Fig. 2(a), this criterion in the 3D Anderson model is a natural consequence of the universal, L-independent shape of its SFF at the transition. As argued in [57], the criterion from Eq. (5) is also consistent with the hybridization condition as a criterion for the EBT as used, e.g., in [56].

The criterion from Eq. (5) is tested in Figs. 4(a) and 4(b) for the numerically extracted values of t_{Th} and t_H. They suggest the EBT to occur at $\alpha \approx \alpha_c = 0.75$, at which t_H/t_{Th} as a function of L is nearly constant [see Fig. 4(a)], and the curves for t_H/t_{Th} at different L, plotted as a function of α, cross at $\alpha = \alpha_c$ [see Fig. 4(b)]. These results are consistent with the universal, L-independent shape of the SFF $K(\tau)$ at $\alpha = \alpha_c$ being the hallmark of the EBT; see Fig. 2(a).

Considering Eq. (4) as a relevant approximation of t_{Th}, one can express the criterion from Eq. (5) as

$$\frac{t_H}{t_{\mathrm{Th}}} = \begin{cases} Ae^{\frac{L}{\xi_0}}, & \alpha > \bar{\alpha} \\ Ae^{-\frac{L}{\xi_1}}, & \alpha < \bar{\alpha} \end{cases}, \tag{6}$$

where the characteristic lengths ξ_0 and ξ_1 in the ergodic ($\alpha > \bar{\alpha}$) and nonergodic ($\alpha < \bar{\alpha}$) regimes, respectively, are defined as

$$\xi_0 = \frac{1}{\ln(\frac{\alpha}{\bar{\alpha}})^2}, \qquad \xi_1 = \frac{1}{\ln(\frac{\bar{\alpha}}{\alpha})^2}. \tag{7}$$

One may think of an inverse of the characteristic lengths, say $1/\xi_0$, as the difference $1/\xi_0 = 1/\xi_\rho - 1/\xi_c$, where $\xi_\rho = 1/\ln(1/\bar{\alpha}^2)$ sets the decay of the mean level spacing and $\xi_c = 1/\ln(1/\alpha^2)$ sets the decay of the weakest coupling to the dot.

We fit the exponential function from Eq. (6), where A and ξ_0 (ξ_1) are fitting parameters, to the numerical results in the main panel in Fig. 4(a). The extracted characteristic lengths ξ_0 and ξ_1 indeed exhibit a tendency to diverge at the transition point α_c. We fit the characteristic length ξ_0 on the ergodic side with a function $c_1/\ln(\alpha/\alpha_c)^2$, where $\alpha_c = 0.75$, and obtain $c_1 = 0.80$. These results are fairly close to the prediction from Eq. (7), which assumes $\alpha_c = \bar{\alpha} = 0.71$ and $c_1 = 1$. We note that despite a reasonably good agreement between numerical results and analytical considerations, the latter may be refined in several ways, which we discuss in [57] in more detail.

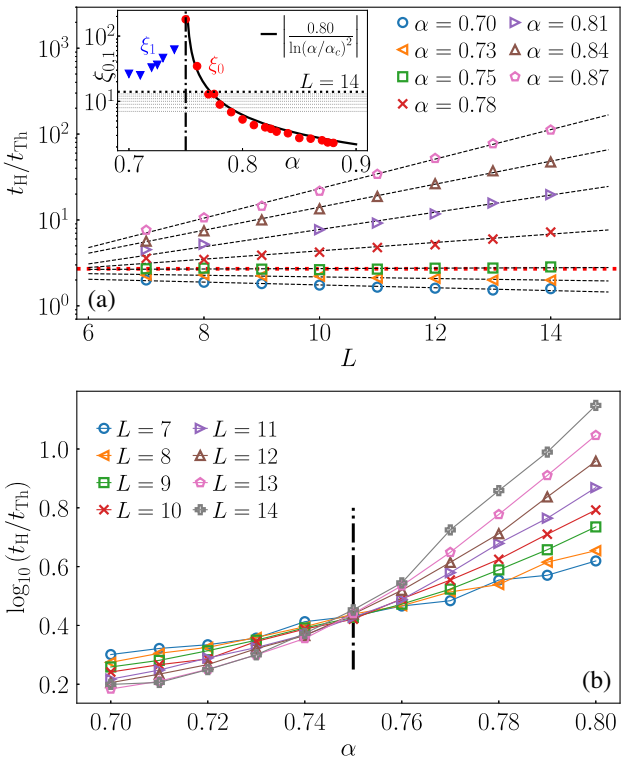

FIG. 4. (a) The ratio t_H/t_{Th} versus L at different α. Symbols are numerical results, while lines are fits of the exponential function from Eq. (6), where A and ξ_0 (ξ_1) are fitting parameters. Inset: characteristic lengths ξ_0, ξ_1, extracted from the fits in the main panel (symbols). Solid line is a one-parameter fit of a function $c_1/\ln(\alpha/\alpha_c)^2$ to ξ_0 in the ergodic regime, where we set $\alpha_c = 0.75$ (vertical dashed-dotted line) and obtain $c_1 = 0.8$ from the fit. The horizontal dashed line denotes $L = 14$, i.e., the largest attainable system size. (b) $\log_{10}(t_H/t_{\mathrm{Th}})$ versus α at different L. Vertical line denotes $\alpha_c = 0.75$.

Conclusions.—In this Letter, we analyzed the model that we suggest to be the toy model of the EBT in a zero-dimensional interacting system. It exhibits three hallmarks of the EBT. The first is a universal, system-size independent form of the SFF at the transition point, which strongly resembles the single-particle SFF of the 3D Anderson model at the localization transition. Determining the analytical form of the universal SFF at the transition, as well as understanding the origin of agreement between the noninteracting 3D Anderson model and the interacting zero-dimensional model studied here, remains an open question for future research.

Another important feature is the exponential scaling of t_{Th} in the ergodic regime with the system size L, where the

rate is a function of the interaction that drives the EBT. In fact, this scaling is observed already deep in the ergodic regime where the level spacing ratio of adjacent gaps r (see [57]) agrees with the GOE prediction, $r \approx 0.53$. To our best knowledge, such a scaling of t_{Th} has so far not been observed in interacting disordered systems in dimension one or higher.

Finally, both analytical arguments and numerical results for the criterion of the EBT show a divergent characteristic length at the transition. This length is, in the vicinity of the transition, much larger than the numerically accessible system sizes L. In the future work it may be instructive to study other measures of the transition that are not based on spectral properties, and to explore their common features.

We acknowledge discussions with W. De Roeck and T. Prosen. This work is supported by the Slovenian Research Agency (ARRS), Research core fundings No. P1-0044 (J. Š. and L. V.) and No. J1-1696 (L. V.). We gratefully acknowledge the High Performance Computing Research Infrastructure Eastern Region (HCP RIVR) consortium [66] and the European High Performance Computing Joint Undertaking (EuroHPC JU) [67] for funding this research by providing computing resources of the HPC system Vega at the Institute of Information Sciences [68].

[1] J. M. Deutsch, Quantum statistical mechanics in a closed system, Phys. Rev. A **43**, 2046 (1991).
[2] M. Srednicki, Chaos and quantum thermalization, Phys. Rev. E **50**, 888 (1994).
[3] M. Srednicki, The approach to thermal equilibrium in quantized chaotic systems, J. Phys. A **32**, 1163 (1999).
[4] M. Rigol, V. Dunjko, and M. Olshanii, Thermalization and its mechanism for generic isolated quantum systems, Nature (London) **452**, 854 (2008).
[5] L. D'Alessio, Y. Kafri, A. Polkovnikov, and M. Rigol, From quantum chaos and eigenstate thermalization to statistical mechanics and thermodynamics, Adv. Phys. **65**, 239 (2016).
[6] J. Eisert, M. Friesdorf, and C. Gogolin, Quantum many-body systems out of equilibrium, Nat. Phys. **11**, 124 (2015).
[7] T. Mori, T. N. Ikeda, E. Kaminishi, and M. Ueda, Thermalization and prethermalization in isolated quantum systems: A theoretical overview, J. Phys. B **51**, 112001 (2018).
[8] J. M. Deutsch, Eigenstate thermalization hypothesis, Rep. Prog. Phys. **81**, 082001 (2018).
[9] M. L. Mehta, *Random Matrices and the Statistical Theory of Spectra*, 2nd ed. (Academic, New York, 1991).
[10] T. Kinoshita, T. Wenger, and S. D. Weiss, A quantum Newton's cradle, Nature (London) **440**, 900 (2006).
[11] M. Gring, M. Kuhnert, T. Langen, T. Kitagawa, B. Rauer, M. Schreitl, I. Mazets, D. A. Smith, E. Demler, and J. Schmiedmayer, Relaxation and prethermalization in an isolated quantum system, Science **337**, 1318 (2012).
[12] T. Langen, S. Erne, R. Geiger, B. Rauer, T. Schweigler, M. Kuhnert, W. Rohringer, I. E. Mazets, T. Gasenzer, and J. Schmiedmayer, Experimental observation of a generalized Gibbs ensemble, Science **348**, 207 (2015).
[13] C. Li, T. Zhou, I. Mazets, H.-P. Stimming, F. S. Møller, Z. Zhu, Y. Zhai, W. Xiong, X. Zhou, X. Chen, and J. Schmiedmayer, Relaxation of bosons in one dimension and the onset of dimensional crossover, SciPost Phys. **9**, 58 (2020).
[14] J. M. Wilson, N. Malvania, Y. Le, Y. Zhang, M. Rigol, and D. S. Weiss, Observation of dynamical fermionization, Science **367**, 1461 (2020).
[15] T. Prosen, Open XXZ Spin Chain: Nonequilibrium Steady State and a Strict Bound on Ballistic Transport, Phys. Rev. Lett. **106**, 217206 (2011).
[16] E. Ilievski, J. De Nardis, B. Wouters, J.-S. Caux, F. H. L. Essler, and T. Prosen, Complete Generalized Gibbs Ensembles in an Interacting Theory, Phys. Rev. Lett. **115**, 157201 (2015).
[17] E. Ilievski, M. Medenjak, T. Prosen, and L. Zadnik, Quasilocal charges in integrable lattice systems, J. Stat. Mech. (2016) 064008.
[18] B. Bertini, F. Heidrich-Meisner, C. Karrasch, T. Prosen, R. Steinigeweg, and M. Žnidarič, Finite-temperature transport in one-dimensional quantum lattice models, Rev. Mod. Phys. **93**, 025003 (2021).
[19] L. F. Santos, Integrability of a disordered Heisenberg spin-1/2 chain, J. Phys. A **37**, 4723 (2004).
[20] O. S. Barišić, P. Prelovšek, A. Metavitsiadis, and X. Zotos, Incoherent transport induced by a single static impurity in a Heisenberg chain, Phys. Rev. B **80**, 125118 (2009).
[21] E. J. Torres-Herrera and L. F. Santos, Local quenches with global effects in interacting quantum systems, Phys. Rev. E **89**, 062110 (2014).
[22] M. Mierzejewski, T. Prosen, and P. Prelovšek, Approximate conservation laws in perturbed integrable lattice models, Phys. Rev. B **92**, 195121 (2015).
[23] B. Bertini, F. H. L. Essler, S. Groha, and N. J. Robinson, Prethermalization and Thermalization in Models with Weak Integrability Breaking, Phys. Rev. Lett. **115**, 180601 (2015).
[24] B. Bertini, F. H. L. Essler, S. Groha, and N. J. Robinson, Thermalization and light cones in a model with weak integrability breaking, Phys. Rev. B **94**, 245117 (2016).
[25] K. Mallayya and M. Rigol, Quantum Quenches and Relaxation Dynamics in the Thermodynamic Limit, Phys. Rev. Lett. **120**, 070603 (2018).
[26] Y. Tang, W. Kao, K.-Y. Li, S. Seo, K. Mallayya, M. Rigol, S. Gopalakrishnan, and B. L. Lev, Thermalization Near Integrability in a Dipolar Quantum Newton's Cradle, Phys. Rev. X **8**, 021030 (2018).
[27] J. Richter, F. Jin, L. Knipschild, H. De Raedt, K. Michielsen, J. Gemmer, and R. Steinigeweg, Exponential damping induced by random and realistic perturbations, Phys. Rev. E **101**, 062133 (2020).
[28] M. Brenes, T. LeBlond, J. Goold, and M. Rigol, Eigenstate Thermalization in a Locally Perturbed Integrable System, Phys. Rev. Lett. **125**, 070605 (2020).
[29] M. Schreiber, S. S. Hodgman, P. Bordia, H. P. Lüschen, M. H. Fischer, R. Vosk, E. Altman, U. Schneider, and I. Bloch, Observation of many-body localization of interacting fermions in a quasi-random optical lattice, Science **349**, 842 (2015).

[30] J. Smith, A. Lee, P. Richerme, B. Neyenhuis, P. W. Hess, P. Hauke, M. Heyl, D. A. Huse, and C. Monroe, Many-body localization in a quantum simulator with programmable random disorder, Nat. Phys. **12**, 907 (2016).
[31] J.-y. Choi, S. Hild, J. Zeiher, P. Schauß, A. Rubio-Abadal, T. Yefsah, V. Khemani, D. A. Huse, I. Bloch, and C. Gross, Exploring the many-body localization transition in two dimensions, Science **352**, 1547 (2016).
[32] A. Lukin, M. Rispoli, R. Schittko, M. E. Tai, A. M. Kaufman, S. Choi, V. Khemani, J. Léonard, and M. Greiner, Probing entanglement in a many-body–localized system, Science **364**, 256 (2019).
[33] S. Scherg, T. Kohlert, P. Sala, F. Pollmann, B. Hebbe Madhusudhana, I. Bloch, and M. Aidelsburger, Observing non-ergodicity due to kinetic constraints in tilted Fermi-Hubbard chains, Nat. Commun. **12**, 4490 (2021).
[34] A. Pal and D. A. Huse, Many-body localization phase transition, Phys. Rev. B **82**, 174411 (2010).
[35] J. Šuntajs, J. Bonča, T. Prosen, and L. Vidmar, Quantum chaos challenges many-body localization, Phys. Rev. E **102**, 062144 (2020).
[36] J. Šuntajs, J. Bonča, T. Prosen, and L. Vidmar, Ergodicity breaking transition in finite disordered spin chains, Phys. Rev. B **102**, 064207 (2020).
[37] P. Sierant, E. G. Lazo, M. Dalmonte, A. Scardicchio, and J. Zakrzewski, Constraint-Induced Delocalization, Phys. Rev. Lett. **127**, 126603 (2021).
[38] T. LeBlond, D. Sels, A. Polkovnikov, and M. Rigol, Universality in the onset of quantum chaos in many-body systems, Phys. Rev. B **104**, L201117 (2021).
[39] D. Sels and A. Polkovnikov, Dynamical obstruction to localization in a disordered spin chain, Phys. Rev. E **104**, 054105 (2021).
[40] D. Sels and A. Polkovnikov, Thermalization of dilute impurities in one dimensional spin chains, arxiv:2105.09348v2.
[41] D. Sels, Signatures of bath-induced quantum avalanches in a many-body–localized system, arxiv:2108.10796v1.
[42] M. Kiefer-Emmanouilidis, R. Unanyan, M. Fleischhauer, and J. Sirker, Evidence for Unbounded Growth of the Number Entropy in Many-Body Localized Phases, Phys. Rev. Lett. **124**, 243601 (2020).
[43] D. J. Luitz and Y. Bar Lev, Absence of slow particle transport in the many-body localized phase, Phys. Rev. B **102**, 100202(R) (2020).
[44] M. Kiefer-Emmanouilidis, R. Unanyan, M. Fleischhauer, and J. Sirker, Slow delocalization of particles in many-body localized phases, Phys. Rev. B **103**, 024203 (2021).
[45] R. Ghosh and M. Žnidarič, Resonance-induced growth of number entropy in strongly disordered systems, Phys. Rev. B **105**, 144203 (2022).
[46] M. Schulz, S. R. Taylor, A. Scardicchio, and M. Žnidarič, Phenomenology of anomalous transport in disordered one-dimensional systems, J. Stat. Mech. (2020) 023107.
[47] P. Sierant, D. Delande, and J. Zakrzewski, Thouless Time Analysis of Anderson and Many-Body Localization Transitions, Phys. Rev. Lett. **124**, 186601 (2020).
[48] D. Abanin, J. Bardarson, G. De Tomasi, S. Gopalakrishnan, V. Khemani, S. Parameswaran, F. Pollmann, A. Potter, M. Serbyn, and R. Vasseur, Distinguishing localization from chaos: Challenges in finite-size systems, Ann. Phys. (Amsterdam) **427**, 168415 (2021).
[49] Á. L. Corps, R. A. Molina, and A. Relaño, Signatures of a critical point in the many-body localization transition, SciPost Phys. **10**, 107 (2021).
[50] M. Hopjan, G. Orso, and F. Heidrich-Meisner, Detecting delocalization-localization transitions from full density distributions, Phys. Rev. B **104**, 235112 (2021).
[51] J. Herbrych, M. Mierzejewski, and P. Prelovšek, Relaxation at different length scales in models of many-body localization, Phys. Rev. B **105**, L081105 (2022).
[52] P. J. D. Crowley and A. Chandran, A constructive theory of the numerically accessible many-body localized to thermal crossover, SciPost Phys. **12**, 202 (2022).
[53] L. Vidmar, B. Krajewski, J. Bonča, and M. Mierzejewski, Phenomenology of Spectral Functions in Disordered Spin Chains at Infinite Temperature, Phys. Rev. Lett. **127**, 230603 (2021).
[54] A. Morningstar, L. Colmenarez, V. Khemani, D. J. Luitz, and D. A. Huse, Avalanches and many-body resonances in many-body localized systems, Phys. Rev. B **105**, 174205 (2022).
[55] P. Sierant and J. Zakrzewski, Challenges to observation of many-body localization, Phys. Rev. B **105**, 224203 (2022).
[56] W. De Roeck and F. Huveneers, Stability and instability towards delocalization in many-body localization systems, Phys. Rev. B **95**, 155129 (2017).
[57] See Supplemental Material, which includes Refs. [58–60], at http://link.aps.org/supplemental/10.1103/PhysRevLett.129.060602 for details about the numerical implementation, comments about the structure of the SFF at the transition and about the hybridization condition as a criterion for the EBT, a discussion about corrections to the analytical expression for Thouless time, and tests of scaling solutions.
[58] V. Oganesyan and D. A. Huse, Localization of interacting fermions at high temperature, Phys. Rev. B **75**, 155111 (2007).
[59] Y. Y. Atas, E. Bogomolny, O. Giraud, and G. Roux, Distribution of the Ratio of Consecutive Level Spacings in Random Matrix Ensembles, Phys. Rev. Lett. **110**, 084101 (2013).
[60] F. Pietracaprina, N. Macé, D. J. Luitz, and F. Alet, Shift-invert diagonalization of large many-body localizing spin chains, SciPost Phys. **5**, 045 (2018).
[61] D. J. Luitz, F. Huveneers, and W. De Roeck, How a Small Quantum Bath can Thermalize Long Localized Chains, Phys. Rev. Lett. **119**, 150602 (2017).
[62] P. J. D. Crowley and A. Chandran, Avalanche induced coexisting localized and thermal regions in disordered chains, Phys. Rev. Research **2**, 033262 (2020).
[63] P. Ponte, C. R. Laumann, D. A. Huse, and A. Chandran, Thermal inclusions: How one spin can destroy a many-body localized phase, Phil. Trans. R. Soc. A **375**, 20160428 (2017).
[64] J. Šuntajs, T. Prosen, and L. Vidmar, Spectral properties of three-dimensional Anderson model, Ann. Phys. (Amsterdam) **435**, 168469 (2021).
[65] K. Slevin and T. Ohtsuki, Critical exponent of the Anderson transition using massively parallel supercomputing, J. Phys. Soc. Jpn. **87**, 094703 (2018).
[66] www.hpc-rivr.si.
[67] eurohpc-ju.europa.eu.
[68] www.izum.si.